Aus der Klinik und Poliklinik für Nuklearmedizin

Klinik der Ludwig-Maximilians-Universität München

Vorstand: Prof. Dr. med. Peter Bartenstein

Microglia-PET imaging as a surrogate marker for post-stroke neuroinflammation in preclinical mouse models and clinical cases: Quantitative PET data analysis using biokinetic modeling and machine learning including information from multiparametric MRI scans

Kumulative Dissertation
zum Erwerb des Doktorgrades der Naturwissenschaften
an der Medizinischen Fakultät der
Ludwig-Maximilians-Universität zu München

vorgelegt von

Artem Zatcepin

aus Voronezh, Russland

2022

Mit Genehmigung der Medizinischen Fakultät

der Universität München

Betreuerin:	Prof. Dr. rer. nat. Sibylle I. Ziegler
Zweitgutachter(in):	Prof. Dr. rer. nat. Guillaume Landry
Dekan:	Prof. Dr. med. Thomas Gudermann
Tag der mündlichen Prüfung:	27. Juni 2023

Eidesstattliche Versicherung

Eidesstattliche Versicherung

Zatcepin, Artem

Name, Vorname

Ich erkläre hiermit an Eides statt, dass ich die vorliegende Dissertation mit dem Titel:

Microglia-PET imaging as a surrogate marker for post-stroke neuroinflammation in pre-clinical mouse models and clinical cases: Quantitative PET data analysis using biokinetic modeling and machine learning including information from multiparametric MRI scans

selbständig verfasst, mich außer der angegebenen keiner weiteren Hilfsmittel bedient und alle Erkenntnisse, die aus dem Schrifttum ganz oder annähernd übernommen sind, als solche kenntlich gemacht und nach ihrer Herkunft unter Bezeichnung der Fundstelle einzeln nachgewiesen habe.

Ich erkläre des Weiteren, dass die hier vorgelegte Dissertation nicht in gleicher oder in ähnlicher Form bei einer anderen Stelle zur Erlangung eines akademischen Grades eingereicht wurde.

München, 30.06.2023
Ort, Datum

Artem Zatcepin
Unterschrift Doktorandin bzw. Doktorand

Content

List of publications

Original publications

This cumulative dissertation is in accordance with the graduation regulation for natural sciences in the medical faculty of the Ludwig-Maximilians-Universität München and based on the following two publications:

Zatcepin, A., Heindl, S., Schillinger, U., Kaiser, L., Lindner, S., Bartenstein, P., ... & Ziegler, S. I. (2022). Reduced Acquisition Time [18F] GE-180 PET Scanning Protocol Replaces Gold-Standard Dynamic Acquisition in a Mouse Ischemic Stroke Model. Frontiers in Medicine, 9. (IF = 5.1)
DOI: 10.3389/fmed.2022.830020.

Zatcepin, A., Kopczak, A., Holzgreve, A., Hein, S., Schindler, A., Duering, M., … & Ziegler, S. I. (2022) ***(in press)***. Machine learning-based approach reveals essential features for simplified TSPO PET quantification in ischemic stroke patients. *Zeitschrift für Medizinische Physik.* (IF = 7.2)

Conference Abstracts

The results of the investigations related to this doctoral thesis were additionally presented at national and international conferences.

Zatcepin, A., Heindl, S., Schillinger, U., Bartenstein, P., Liesz, A., & Ziegler, S. (2021). Can static F-18-GE180 PET be a sufficient surrogate marker for post-stroke neuroinflammation in a mouse model? Nuklearmedizin-NuclearMedicine April 14-17, 2021 Virtual, 60(02): 178-179, P32.
DOI: 10.1055/s-0041-1726846

Zatcepin, A., Kopczak, A., Holzgreve, A., Duering, M., Kaiser, L., Schidlowski, M., Stoecker, T., Bartenstein, P., Dichgans, M., Brendel, M., & Ziegler, S. (2021). Voxelwise Distribution Volume Prediction Using Random Forest. PET is Wonderful Annual Meeting October 26, 2021 Virtual.

Zatcepin, A., Xiang, X., Parhizkar, S., Gnörich, J., Grosch, M., Wind, K., ... & Brendel, M. (2022). Desynchronization of microglial activity is closely associated with cognitive decline in Alzheimer's disease. Nuklearmedizin-NuclearMedicine April 27-30, 2022 Leipzig, Germany, 61(02): 151-152, L43.
DOI: 10.1055/s-0042-1745982

Zatcepin, A., Xiang, X., Parhizkar, S., Gnoerich, J., Grosch, M., Wind, K., ... & Brendel, M. TREM2 Deficiency Desynchronises Microglial Activity in the Mouse Brain. European Association of Nuclear Medicine October 20-23, 2021 Virtual. *Eur J Nucl Med Mol Imaging* **48** (Suppl 1), S130-S131 (2021).
DOI: 10.1007/s00259-021-05547-1

Zatcepin, A., Xiang, X., Parhizkar, S., Gnörich, J., Grosch, M., Wind, K., Shi, Y., Beyer, L., Biechele, G., Eckenweber, F., Wiedemann, T., Rauchmann, B.-S., Lindner, S., Rominger, A., Bartenstein, P., Willem, M., Tahirovic, S., Herms, J., Haass, C., . . . Brendel, M. (2022). Regional Desynchronization of Microglial Activity is Associated with Cognitive Decline in Alzheimer's Disease. SNMMI Annual Meeting June 11-14, 2022 Vancouver, Canada. *Journal of Nuclear Medicine*, 63 (supplement 2), 2953.

Zatcepin, A., Kopczak, A., Holzgreve, A., Schindler, A., Duering, M., Kaiser, L., ... & Ziegler, S. (2022). Machine learning-based approach reveals essential features for simplified TSPO PET

quantification in ischemic stroke patients. European Association of Nuclear Medicine October 15-19, 2022 Barcelona, Spain. *Eur J Nucl Med Mol Imaging* **49** (Suppl 1), S618-S619 (2022).
DOI: 10.1007/s00259-022-05924-4

Further publications

Within the scope of the investigations related to this doctoral thesis, contributions to the following publication were made:

Zatcepin, A., & Ziegler, S. I. (2022). Detectors in positron emission tomography. *Zeitschrift für Medizinische Physik*. (IF = 7.2)
DOI: 10.1016/j.zemedi.2022.08.004

Zatcepin, A., Pizzichemi, M., Polesel, A., Paganoni, M., Auffray, E., Ziegler, S. I., & Omidvari, N. (2020). Improving depth-of-interaction resolution in pixellated PET detectors using neural networks. Physics in Medicine & Biology, 65(17), 175017. (IF = 4.2)
DOI: 10.1088/1361-6560/ab9efc

Xiang, X., Wind, K., Wiedemann, T., Blume, T., Shi, Y., Briel, N., … **Zatcepin, A.**, ... & Brendel, M. (2021). Microglial activation states drive glucose uptake and FDG-PET alterations in neurodegenerative diseases. Science translational medicine, 13(615), eabe5640. (IF = 19.3)
DOI: 10.1126/scitranslmed.abe5640

Reifschneider, A., Robinson, S., van Lengerich, B., Gnörich, J., Logan, T., Heindl, S., … **Zatcepin, A.**, ... & Haass, C. (2022). Loss of TREM2 rescues hyperactivation of microglia, but not lysosomal deficits and neurotoxicity in models of progranulin deficiency. The EMBO Journal, e109108. (IF = 13.8)
DOI: 10.15252/embj.2021109108

Xia, D., Lianoglou, S., Sandmann, T., Calvert, M., Suh, J. H., Thomsen, E., ... **Zatcepin, A.**, … & Sanchez, P. E. (2022). Novel App knock-in mouse model shows key features of amyloid pathology and reveals profound metabolic dysregulation of microglia. Molecular neurodegeneration, 17(1), 1-29. (IF = 18.9)
DOI: 10.1186/s13024-022-00547-7

Bartos, L. M., Kirchleitner, S. V., Blobner, J., Wind, K., Kunze, L. H., Holzgreve, A., ..., **Zatcepin, A.**, …, & Brendel, M. (2022). 18 kDa translocator protein positron emission tomography facilitates early and robust tumor detection in the immunocompetent SB28 glioblastoma mouse model. Frontiers in medicine, 2848. (IF = 5.1)
DOI: 10.3389/fmed.2022.992993

Abbreviations

3D	three-dimensional
AD	Alzheimer's disease
ADC	apparent diffusion coefficient
AIC	Akaike information criterion
AIF	arterial input function
ASL	arterial spin labeling
BBB	blood-brain barrier
CBF	cerebral blood flow
CBWM	cerebellar white matter
CCC	concordance correlation coefficient
CSF	cerebrospinal fluid
CT	computed tomography
DCE	dynamic contrast enhanced
DSC	dynamic susceptibility contrast
DVR	distribution volume ratio
DWI	diffusion-weighted imaging
FA	factor analysis
FDG	[18F]Fluorodeoxyglucose
FLAIR	fluid-attenuated inversion and recovery
FOV	field of view
HAB	high-affinity binder
IDIF	image-derived input function
IF	input function
LAB	low-affinity binder
LD	labeling delay
MAB	mixed-affinity binder
MITK	Medical Imaging Interaction Toolkit
ML	machine learning
MNI	Montreal Neurological Institute
MR	magnetic resonance
MRI	magnetic resonance imaging
OSEM	ordered subset expectation maximization
p.i.	post injection
PET	positron emission tomography
PLD	postlabeling delay
PT	photothrombotic stroke
PVE	partial volume effect
RF	random forest

ROI	region of interest
SD	standard deviation
SHAP	Shapley additive explanations
SNR	signal-to-noise ratio
SPM	Statistical Parametric Mapping
SUV	standardized uptake value
SUVR	standardized uptake value ratio
TAC	time-activity curve
TE	echo time
TI	inversion time
TR	repetition time
TSPO	18 kDa translocator protein
VOI	volume of interest
V_T	volume of distribution
WHO	world health organization

1. Contribution to the publications

1.1 Contribution to the first publication

The first publication included 48 [^{18}F]GE-180 positron emission tomography–magnetic resonance imaging (PET/MR) mouse scans. First, I reconstructed the PET scans using Nucline^{TM} acquisition software (Mediso Ltd, Hungary). The reconstruction was performed with an ordered subset expectation maximization 3D-based (OSEM-3D-based) algorithm (Tera-Tomo^{TM}, Mediso Ltd, Hungary). For attenuation correction I used the corresponding T1-weighted MR image. For each image, a body-air threshold used for the material map creation was manually checked and adjusted to ensure that the resulting segmentation covers the head of the mouse as closely as possible.

Next, I performed all the image pre-processing steps that included cropping of the brain region in both PET and MR images; deformable registration (SPM5 procedure) of MR images to a high-resolution MR template that included affine transformation and warping; segmentation of the cerebellum and cortex volume of interest (VOI) using the Ma-Benveniste-Mirrione atlas; definition of a cerebellar white matter VOI; dilation of a photothrombotic stroke (PT) VOI defined by Dr. S. Heindl by 1 mm at all borders to include microglia possibly located in the peri-lesional area. For this, I used PMOD View and FuseIt tools (version 4.005, PMOD Technologies, Zurich, Switzerland).

After that, I generated an image-derived input function (IDIF), for which, inspired by the paper from Wimberley et al (Wimberley et al., 2020), I developed a procedure called factor analysis-based partial volume effect correction. The procedure included (1) cropping of the vena cava region using PMOD View, (2) factor analysis on the cropped image using Pixies (Apteryx, France), (3) multiplication of the blood factor curve with the corresponding factor image, (4) automatic segmentation of a VOI in the resulting image for the IDIF definition, (5) time-activity curve (TAC) extraction, (6) TAC fitting using the 2-exponential linear model in PMOD Kinetic. Steps 3 through 5 were performed using a custom Python script that I wrote by myself using SimpleITK, NiBabel, Pandas, and NumPy packages.

Using the generated IDIF, I performed kinetic modeling with Logan plot by means of PMOD Kinetic. I created another Python script using SciPy, Pingouin, NumPy, and Pandas libraries to (1) correlate distribution volume ratio (DVR) and standardized uptake value (SUV) ratio in PT VOI in the analysis cohort, (2) estimate DVR in the PT VOI in the validation cohort using the fits calculated for the analysis cohort, (3) perform statistical analysis. I created all the figures in the manuscript using Matplotlib (Python), PMOD, and PowerPoint.

I wrote the first draft of the paper on my own, which was then corrected and extended by my co-authors. As both the first and the corresponding author of the paper, I was responsible for the submission and revision process as well as for the communication with the journal.

1.2 Contribution to the second publication

I performed all ischemic lesion segmentations using the Medical Imaging Interaction Toolkit (MITK) Workbench, which were then checked and, when needed, corrected by an experienced neuroradiologist. I performed all the image spatial co-registration steps described in the paper (PMOD FuseIt, Neuro). I wrote a Python script to create the mask described in Section 2.5 of the

manuscript using SimpleITK and NumPy libraries. PET reconstructions were also partially performed by me.

I performed all the steps related to input function generation: (1) gamma counter measurements of activity of venous blood and plasma drawn by a physician at five timepoints as well as gamma counter cross-calibration with the PET/computed tomography (CT) scanner; (2) creating a Python script (SimpleITK, NiBabel, Pandas libraries) for automated segmentation of carotid arteries, TAC extraction, fitting, calibration, and metabolite correction.

Next, I created a Python script for voxelwise 18 kDa translocator protein (TSPO) binding prediction in the study patients. The script incorporated Scikit-learn implementation of the random forest algorithm. Additionally, I implemented the Logan plot analysis in Python (SciPy, NumPy libraries) for automated voxelwise PET quantification to generate ground truth for the machine learning algorithm. Lastly, in Python I calculated Shapley additive explanations (SHAP library), performed reduced-features model comparison, and statistical tests (Pingouin library). I created all the figures in the manuscript using Matplotlib (Python), PMOD, and PowerPoint.

I drafted the first version of the manuscript, which was then iteratively refined together with my co-authors. Being both the first and the corresponding author of the paper, I handled the submission process, coordinated the revision process, and was responsible for the communication with the journal.

2. Introduction

2.1 Overview

Stroke is the second-leading cause of death and the third-leading cause of death and disability combined worldwide (Feigin et al., 2022). Therefore, post-stroke recovery remains a huge research topic worldwide. Microglia activation is thought to be one of the key factors influencing the recovery process, and multiple studies were performed to access its extent after acute ischemic stroke (Ma et al., 2017). Activated microglia are known to have a high expression level of the 18 kDa tranlocator protein (TSPO) (Knezevic & Mizrahi, 2018; Vivash & O'Brien, 2016). TSPO positron emission tomography (PET) is a technique that provides *in-vivo* assessment of microglia activation (Ma et al., 2017). Several TSPO PET tracers have been developed over the years, including [^{18}F]GE-180, and existing kinetic modeling approaches enable quantitative estimation of TSPO binding from [^{18}F]GE-180 PET images (Fan et al., 2016). Yet, these gold-standard methods are burdensome and not feasible to implement for a common nuclear medicine department and cause discomfort to the patient, which explains the need for a simplified quantification approach.

2.2 Objective of this thesis

This thesis aimed at establishing a simplified TSPO quantification approach using a short late [^{18}F]GE-180 PET acquisition (Figure 1). The first step was to create and evaluate the quantification method in a mouse model of ischemic stroke (Figure 1A, Paper 1), the second step was to adjust it to a human ischemic stroke dataset and, by means of machine learning (ML), determine whether incorporating additional information such as plasma activity concentration at various timepoints and brain perfusion from arterial spin labeling (ASL) magnetic resonance (MR) images improves the performance of the algorithm (Figure 1B, Paper 2).

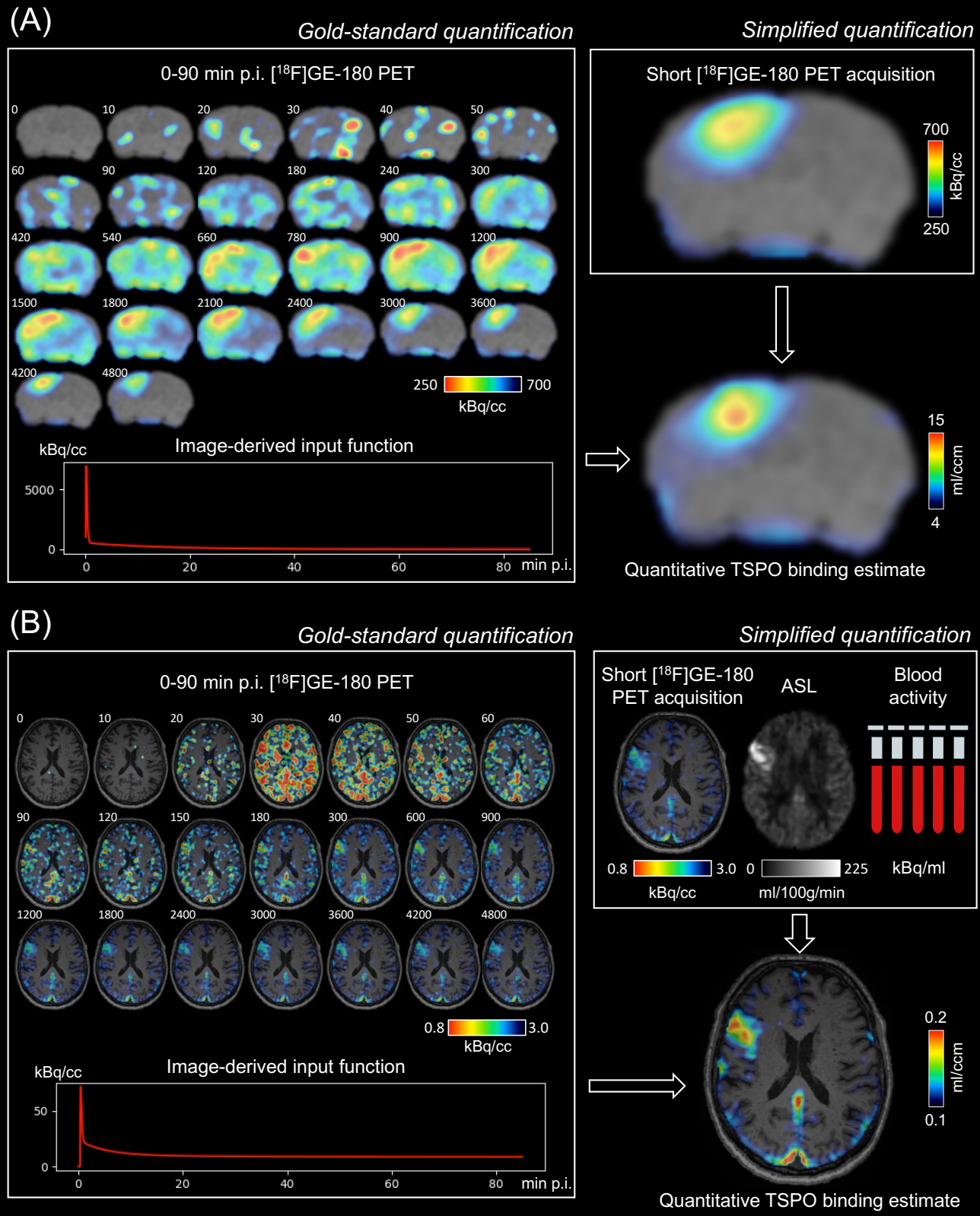

Figure 1. Thesis objective. (A) Mouse study. (B) Human study. TSPO quantification in both mice and humans requires a 0-90 min p.i. PET acquisition and an arterial input function (can be replaced by an image-derived input function) (*left*). The goal of this dissertation was to establish a quantification approach based on a short [^{18}F]GE-180 PET acquisition (*right*). For the human study (B), we additionally tested whether ASL-derived brain perfusion and activity of blood samples drawn after the tracer injection improves the estimation. The numbers next to PET images indicate frame start time in seconds p.i. PET images are shown on top of T1w MR images for better visualization.

2.3 Ischemic stroke

An ischemic stroke, or cerebral infarction, is caused by reduced blood supply to the brain tissue. First, this results in transient functional loss in the brain tissue. Ischemia then triggers a chain of processes including electrical function loss, calcium influx-induced excitotoxicity, and formation of reactive oxygen species, which eventually leads to severe cell membrane damage and cell death (Feske, 2021). The most common causes of ischemic stroke are cardioembolism, artery-to-artery embolism, paradoxical embolism, large vessel disease, atherosclerotic stenosis of occlusion, small vessel disease (Feske, 2021).

In most clinics, a noncontrast head computed tomography (CT) is performed to identify ischemic stroke due to its availability and speed. On the CT, one needs to search for gray-white matter differentiation loss, which could be caused by reduced density in, e.g., the insular cortex or the deep gray matter (Feske, 2021). Additionally, the CT scan provides a sensitive means to exclude hemorrhage (Herpich & Rincon, 2020). Later, mass effect is observed, which can be seen by sulcal effacement, as well as frank hypodensity (Feske, 2021).

MR imaging (MRI) provides a more precise way of identifying ischemic stroke compared to CT. With MRI sequences such as diffusion-weighted imaging (DWI) and apparent diffusion coefficient (ADC), acute cerebral infarction is diagnosed with an accuracy of up to 100%. Within the first 6 hours after the onset, a typical ischemic stroke lesion is hyper-intense on DWI, hypo-intense on ADC, and not yet visible on fluid-attenuated inversion and recovery (FLAIR) MRI (Feske, 2021).

Further assessments might require perfusion CT or perfusion MR. Perfusion MRI techniques include dynamic susceptibility contrast (DSC), dynamic contrast enhanced (DCE), and ASL. Perfusion CT as well as DWI are used to estimate the extent of irreversibly damaged brain tissue (Powers, 2020). Perfusion CT and perfusion MRI are used to determine the penumbra, ischemic brain tissue that with high probability can be recovered, which is seen by delayed arrival of contrast. CT angiography and MR angiography are employed to define sites of intracranial arterial occlusions in order to perform thrombectomy (Nogueira et al., 2018; Powers, 2020).

2.3.1 The role of microglia in ischemic stroke

Neuroinflammation is a crucial component of ischemic stroke pathophysiology (Moskowitz et al., 2010). Brain inflammatory response starts with the activation of microglia, resident brain immune cells, which can occur within minutes after cerebral infarction (Nakajima & Kohsaka, 2004). Several studies showed the presence of activated microglia at the acute (Krupinski et al., 1996; Tomimoto et al., 1996), the subacute (Price et al., 2006), and the recovery phase (Gulyás et al., 2012). PET studies demonstrated that microglia activation remains high in the peri-infarct zone longer than in the infarct zone (Gulyás et al., 2012) and that microglia can spread from the stroke site into connected regions at the recovery stage (Gerhard et al., 2005).

Activated microglia produce a wide range of mediators, which can enhance or inhibit neuronal damage (Ma et al., 2017). It was shown that activated microglia in the infarct zone are associated with negative clinical outcome (Thiel et al., 2010). There they can aggravate delayed death of neurons by generating toxic substances (Ma et al., 2017). However, activated microglia produce growth factors and can therefore enhance neuronal regeneration (Madinier et al., 2009). Moreover, microglial cells clean the infarct area by removing cellular debris (Stoll et al., 1998). These studies suggest that microglia is a promising intervention target to improve post-stroke recovery (Thiel & Heiss, 2011).

2.4 Positron emission tomography (PET)

PET is an imaging technique that enables in-vivo estimation of various metabolic processes and density quantification of a wide range of cellular receptors, which is achieved by injecting into the patient's bloodstream a radioactive-labeled substance taking part in a metabolic process under investigation. This substance is called tracer. PET tracers are always labeled with β^+-emitters. The decay of such isotopes results in generation of a positron, which, after traveling a short distance within the tissue called positron range, annihilates with a tissue electron. This generates two 511 keV annihilation photons propagating in opposite directions. The photon pair is then detected by PET detectors arranged in a ring and consisting of a scintillation crystal that converts the energy of the annihilation photons into visible light and a photomultiplier that amplifies the detected signal. Detection of photon pairs spreading in opposite directions eliminates the need for a physical collimator. The location of the annihilation event is determined down to the line between the two scintillators where the photons were detected, or line of response. This is called electronic collimation. The two annihilation photons must be detected within a predefined coincidence time window to be recorded as a coincidence. All the coincidence events recorded during the scan, or list-mode data, can be reconstructed either together as a single image (static reconstruction) or can be first split into several pre-defined time frames, which are reconstructed individually (dynamic reconstruction). The latter provides the information on tracer behavior in time and is required for tracer kinetic modeling. PET images are usually reconstructed using either filtered backprojection or iterative algorithms such as ordered subset expectation maximization (OSEM). During the reconstruction process, several corrections are made, which include corrections for physical decay of the tracer, annihilation photons originating from different decays but detected within the coincidence time window, and attenuation by the imaged object and the bed (Cherry et al., 2012).

2.4.1 Tracer kinetic modeling for quantitative PET

PET enables imaging of metabolic processes or specific receptor molecules, which is achieved by selecting an appropriate radioligand. For instance, intensity of glucose uptake and phosphorylation can be estimated by measuring the uptake of fluorodeoxyglucose ([^{18}F]FDG), a glucose analog, which is absorbed by the cell and phosphorylated but cannot be further metabolized and remains trapped in the cell (Ido et al., 1978; Pauwels et al., 1998). Other examples include beta amyloid imaging using tracers such as [^{11}C]Pittsburgh Compound-B and [^{18}F]Florbetapir for early diagnostics of Alzheimer's disease (AD) (Suppiah et al., 2019) and TSPO imaging using tracers such as [^{11}C]PK11195, [^{11}C]ER176, [^{18}F]GE-180 to assess the level of neuroinflammation (Werry et al., 2019).

However, tracer signal in PET images originates not only from the tracer at a metabolic site of interest or specifically bound tracer in the target tissue. Depending on the tracer, these values can be contaminated by unspecifically bound tracer in the target tissue, free tracer in the target tissue and blood, tracer bound to plasma proteins, and metabolized tracer. Quantification of specifically bound tracer can be performed via kinetic modeling.

A kinetic model is a mathematical approximation that links the dynamics and possible states (called compartments) of the tracer to the final PET image. By knowing the tracer dynamics provided by PET acquisition starting directly at tracer injection time and followed by multi-frame reconstruction, all the possible tracer states, and ways of conversion between them, one can isolate the signal of interest (Morris et al., 2004). In many receptor studies, the endpoint of kinetic analysis

is the volume of distribution (V_T), which is the ratio of the tracer concentration in the target tissue to its concentration in plasma (Innis et al., 2007).

2.4.1.1 Compartment models

One of the simplest kinetic models is the one-tissue compartment model (Gunn et al., 2001). This model only separates tracer uptake by the target tissue (K_1, ml/ccm/min) and its washout (k_2, 1/min) (Figure 2A).

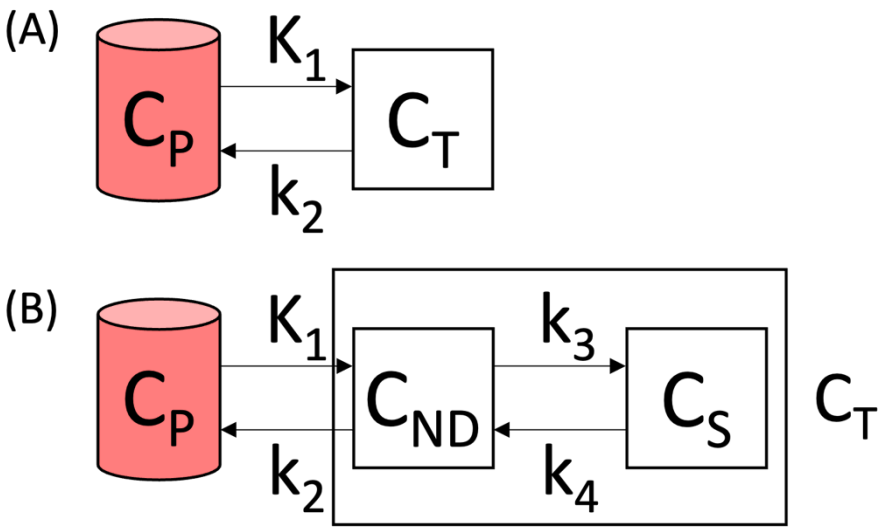

Figure 2. Compartment models. (A) One-tissue compartment model. (B) Two-tissue compartment model. C_P is the free tracer concentration in arterial plasma, C_T is the tracer concentration in the target tissue, C_{ND} is the non-displaceable tracer concentration in the tissue, C_S is the concentration of specifically bound tracer in the tissue. K_1, k_2, k_3, and k_4 are kinetic constants.

The differential equation of the mass balance for this model is written as follows:

$$\frac{dC_T(t)}{dt} = K_1 C_P(t) - k_2 C_T(t), \tag{1}$$

where $C_T(t)$ is the tracer concentration in the target tissue and $C_P(t)$ is the free tracer concentration in arterial plasma. Its solution is a convolution of $C_p(t)$ and the impulse response function, which for the one-tissue model is $K_1 e^{-k_2 t}$ (Gunn et al., 2001):

$$C_T(t) = C_P(t) \otimes K_1 e^{-k_2 t}.$$

Considering that

$$C_{PET}(t) = (1 - V_B) C_T(t) + V_B C_B(t), \tag{2}$$

where $C_{PET}(t)$ is the tracer uptake value from the PET image, $C_B(t)$ is the tracer concentration in blood, V_B is the ratio of blood volume to the total volume of the target tissue, one can estimate V_T as follows (Innis et al., 2007):

$$V_T = \frac{K_1}{k_2}. \tag{3}$$

A more complex compartment model is the two-tissue compartment model (Gunn et al., 2001), which additionally separates C_T into two compartments: free and non-specifically bound tracer in

the target tissue (non-displaceable compartment, C_{ND}) and specifically bound tracer (C_S) (Figure 2B). The model includes two additional rate constants, k_3 (1/min) and k_4 (1/min), depicting the exchange between these two compartments. To determine V_T, one needs to solve the differential equations of the mass balance

$$\frac{dC_{ND}(t)}{dt} = K_1 C_P(t) - (k_2 + k_3) C_{ND}(t) + k_4 C_S(t),$$

$$\frac{dC_S(t)}{dt} = k_3 C_{ND}(t) - k_4 C_S(t),$$

together with equation (2). V_T is then calculated as follows (Innis et al., 2007):

$$V_T = \frac{K_1}{k_2}\left(1 + \frac{k_3}{k_4}\right). \quad (5)$$

Kinetic modeling with more than two compartments is possible (Gunn et al., 2001); however, the practical use of such models is limited due to the high number of parameters that have to be fitted.

2.4.1.2 Logan plot graphical analysis

Logan plot offers a simplified way of calculating V_T. Compared to compartment models, it reduces the number of fitting parameters to two and replaces non-linear fitting by linear fitting, which provides more robust results and is less computationally expensive. The Logan plot equation is obtained by rearranging compartmental equations for an arbitrary number of compartments (Gunn et al., 2001; Logan et al., 1990) and integrating them and is written as follows:

$$\frac{\int_0^t C_T(\tau)d\tau}{C_T(t)} = \mathrm{V_T}\frac{\int_0^t C_P(\tau)d\tau}{C_T(t)} + b, \quad (6)$$

where b is the intercept. Linear fitting is then performed for the two fraction terms, the slope of the fit line is V_T (Logan et al., 1990).

2.4.1.3 Input function (IF)

C_P, or arterial IF, is estimated directly by either continuous measurement of arterial blood radioactivity (Watabe et al., 2006), which is performed by means of an external detector (Boellaard et al., 2001; Eriksson et al., 1988) and/or by measuring frequently drawn manual arterial samples (Watabe et al., 2006). There exist several non-invasive methods of IF estimation, such as population-based IF (Buchert et al., 2020), image-derived IF (Mourik et al., 2009), and factor analysis (Wimberley et al., 2020). Depending on the tracer and the method, following corrections might be required for the IF: plasma-to-whole-blood ratio, plasma metabolite correction, plasma protein correction.

2.4.2 TSPO PET

The 18 kDa translocator protein (TSPO) is primarily expressed on the outer mitochondrial membrane (Guilarte, 2019). Under physiological conditions, highest TSPO expression levels are observed in steroidogenic tissues, while its expression in central nervous system is relatively low (Papadopoulos et al., 2006). However, neuroinflammation leads to a pronounced increase of TSPO expression in activated microglia (Knezevic & Mizrahi, 2018; Vivash & O'Brien, 2016) and reactive astrocytes (Lavisse et al., 2012), which suggested a possible use of TSPO in assessing

the outcome of anti-inflammatory interventions (Gershen et al., 2015; Setiawan et al., 2015; Zhang et al., 2021).

Multiple TSPO radiotracers have been developed over the years. The first TSPO tracer, [^{11}C]PK11195, is also the one that has been most extensively applied for neuroinflammation imaging in various neurological disorders (Morris et al., 2018; Sucksdorff et al., 2017; Zhang et al., 2021). [^{11}C]PK11195, however, has important disadvantages, such as low signal-to-noise ratio (SNR) and short physical half-life, the latter limiting its use to medical facilities with an on-site cyclotron (Zhang et al., 2021). Second-generation TSPO tracers demonstrated enhanced SNR, but it was discovered that these tracers have variable TSPO binding affinity in different human subjects due to a single-nucleotide polymorphism (rs6971) in human TSPO gene (Fan et al., 2015; Kreisl et al., 2013). An individual can be homozygous for high-affinity state (high-affinity binder, HAB), homozygous for low-affinity state (low-affinity binder, LAB), or heterozygous (mixed-affinity binder, MAB) (Kreisl et al., 2013). Third-generation TSPO tracers have lower sensitivity to the rs6971 polymorphism (Zhang et al., 2021) and include [^{18}F]FEBMP (Tiwari et al., 2014), [^{18}F]GE-180 (Fan et al., 2016), [^{11}C]ER176 (Ikawa et al., 2017), and [^{18}F]GE387 (Qiao et al., 2019).

2.4.3 Properties and kinetic modeling of [^{18}F]GE-180

[^{18}F]GE-180 is a third-generation TSPO tracer with excellent TSPO binding, high brain absorption affinity (Wadsworth et al., 2012), higher SNR (Boutin et al., 2015), and longer physical half-life compared to [^{11}C]PK11195. Feeney et al. observed no effect of the rs6971 polymorphism on K_1, V_T, distribution volume ratio (DVR), standardized uptake value (SUV), and SUV ratio when comparing HABs and MABs (Feeney et al., 2016). Even at late timepoints after the injection, [^{18}F]GE-180 has a high parent fraction (Fan et al., 2016; Feeney et al., 2016). However, low brain absorption of [^{18}F]GE-180 in healthy human subjects was reported (Zanotti-Fregonara et al., 2018).

[^{18}F]GE-180 has been extensively used to monitor neuroinflammation in various animal models, including ischemic stroke (Boutin et al., 2015; Chaney et al., 2019), AD (Deussing et al., 2018; Liu et al., 2015; López-Picón et al., 2018), glioblastoma (Holzgreve et al., 2022), epilepsy (Brackhan et al., 2018; Russmann et al., 2017), as well as in a number of clinical trials, e.g. in glioma (Albert et al., 2017; Kaiser et al., 2022; Unterrainer et al., 2020), multiple sclerosis (Unterrainer et al., 2018; Vomacka et al., 2017), AD, four-repeat tauopathy (Vettermann et al., 2021), corticobasal syndrome (Schuster et al., 2022), and progressive multifocal leukoencephalopathy (Mahler et al., 2021) patients.

2.4.3.1 Kinetic modeling approaches of [^{18}F]GE-180

Fan et al. tested five compartment models for kinetic modeling of [^{18}F]GE-180: one-tissue model (Figure 2A), one-tissue model with an extra vascular component, two-tissue model (Figure 2B), two-tissue model with an extra vascular component, and two-tissue model with irreversible binding ($k_4 = 0$), on ten healthy subjects (6 HAB, 4 MAB) (Fan et al., 2016). The two-tissue model demonstrated the best performance among the investigated models – it yielded the lowest Akaike information criterion (AIC) (Akaike, 1974) for tested volumes of interest (VOIs), smallest coefficient of variation of V_T, lowest weighted residual sum square, and more random residual sequence as shown by the Wald-Wolfowitz test. The authors also showed a strong positive correlation between the two-tissue model-derived V_T and Logan plot-derived V_T.

Feeney et al reported similar results: the authors tested the one- and two-tissue compartment model on ten healthy subjects (5 HAB, 5 MAB) and showed that the two-tissue model had lower AIC in most of the studied VOIs (Feeney et al., 2016). Adding V_B as a fitting parameter to the two-tissue model did not improve the results compared to the model with V_B fixed at 5%. Similar to Fan et al., the authors reported a strong correlation between V_T estimates from two-tissue compartment model and Logan plot.

However, these approaches require 90 min PET scan and arterial IF. Therefore, simplified methods are needed.

2.5 Magnetic resonance imaging (MRI)

MRI is an imaging technique that provides detailed structural information with high soft tissue contrast. It is based on magnetic resonance of hydrogen atoms nuclei (^{1}H) of the imaged tissue. In the presence of a strong static magnetic field (B_0, 1-10T), the nuclear spins within the tissue become aligned and start to precess with the Larmor frequency, which generates net magnetization. Next, a radiofrequency magnetic field (B_1, several μT) is applied to disturb the thermal equilibrium. The nuclear spins then return to the thermal equilibrium in the process called relaxation, which can be divided into longitudinal and transversal relaxation. The longitudinal (T1) and transversal relaxation time (T2) are tissue-dependent and therefore can provide tissue contrast (Weishaupt & Köchli, 2009).

2.5.1 Arterial spin labeling (ASL)

ASL is a quantitative MR-based perfusion imaging technique that does not require contrast media. ASL is performed in two acquisitions. For the first, or labeled, acquisition, magnetic labeling of protons in arterial blood at the neck vessels, i.e., upstream from the volume to be imaged, by means of radiofrequency pulses is performed. The image is then obtained after the labeled protons have perfused the imaged tissue. The second, or control, acquisition is performed without the labeling. The perfusion-weighted image is then derived by subtracting the control image from the labeled image (Ferré et al., 2013). It is possible to generate a quantitative cerebral blood flow (CBF) map from the perfusion-weighted image (ΔM) by applying a kinetic model (Buxton et al., 1998; Ferré et al., 2013):

$$\Delta M = 2M_{a,0} \cdot CBF \cdot \int_0^t c(\tau) r(t-\tau) m(t-\tau) d\tau,$$

where $M_{a,0}$ is the equilibrium magnetization in a voxel of arterial blood, $c(t)$ is the normalized concentration of magnetization in arterial blood, $r(t-\tau)$ is the output of the labeled protons from the voxel, and $m(t-\tau)$ represents the impact of longitudinal relaxation.

The main advantages of ASL include the lack of ionizing radiation and contrast medium, possibility of absolute CBF quantification and repeated measurements, and high reproducibility. The main disadvantages of ASL are low SNR and spatial resolution (Ferré et al., 2013).

2.6 Machine learning (ML)

ML comprises mathematical algorithms that create a model based on training data to make predictions without being explicitly programmed (Koza et al., 1996). If training data include not only

inputs but also desired outputs, a ML learning algorithm is called supervised (Russell, 2010). Examples of ML models include artificial neural networks, decision trees, and support-vector machines. In recent years, ML methods have been successfully implemented for a variety of medical imaging problems, such as image segmentation (Seo et al., 2020), classification (Vandenberghe et al., 2013), reconstruction (G. Wang et al., 2020), attenuation correction (T. Wang et al., 2020) and IF estimation in PET (Kuttner et al., 2020; Kuttner et al., 2021). When used for quantitative PET analysis, ML can provide more robust parameter estimation (Pan et al., 2017).

2.6.1 Random forest

Decision trees are a supervised ML technique that is based on splitting the input data according to certain conditions (Maimon & Rokach, 2014). The splitting process occurs at decision nodes, while decision leaves contain the final results.

Several ML models can be combined for improved prediction accuracy compared to any of the composing models alone. This approach is called ensemble learning (Polikar, 2006). Random forest is an ensemble learning approach that builds multiple decision trees at training time. When used for regression tasks, the method outputs mean prediction of the constituent trees (Ho, 1995). Random forest is much less prone to overfitting compared to an individual decision tree (Hastie et al., 2009). In the second paper of this dissertation, random forest was used for estimating V_T.

2.6.2 Shapley additive explanations

Shapley additive explanations (SHAP) (Lundberg & Lee, 2017) is a method to estimate the impact of individual input features on the model predictions that can be applied to any ML model. The method computes a Shapley value (Shapley, 1997) for each feature of the investigated sample, which corresponds to the feature's impact, by using Kernel Shap, a simplified calculation approach based on local interpretable model-agnostic explanations (LIME) (Ribeiro et al., 2016). In the second paper of this dissertation, SHAP were used to assess the importance of individual features on V_T predictions.

3. Zusammenfassung

Hintergrund

Der ischämische Schlaganfall ist weltweit die zweithäufigste Todesursache und die dritthäufigste Ursache für Langzeitbehinderungen, was den Bedarf an neuartigen Therapien zur Verbesserung der neurologischen Erholung erklärt. Mikroglia, Immunzellen im Gehirn, sind ein geeignetes Ziel für eine solche Therapie. Diese Zellen exprimieren das 18 kDa-Translokatorprotein (TSPO), wenn sie aktiviert sind, was die Messung von Neuroinflammation mittels Positronen-Emissions-Tomographie (PET) mit TSPO-Tracern wie [^{18}F]GE-180 ermöglicht. Das Signal in den PET-Bildern stammt jedoch nicht nur von der spezifischen Bindung des Tracers an den betreffenden Rezeptor, sondern wird auch durch unspezifische Bindungen und freien Tracer im Gewebe und im Blut kontaminiert. Die Goldstandard-Quantifizierung der spezifischen Bindung von [^{18}F]GE-180 wird derzeit mit Hilfe pharmakokinetischer Modelle durchgeführt, was eine längere Messzeit und eine kontinuierliche arterielle Blutentnahme erfordert. Dies ist nicht nur für das Krankenhauspersonal belastend, sondern auch mit zusätzlichen Risiken und Unannehmlichkeiten für die Patienten verbunden.

Zielsetzung

Ziel dieser Arbeit war es, ein vereinfachtes [^{18}F]GE-180-PET-Scanprotokoll für ein ischämisches Schlaganfallmodell bei Mäusen zu erstellen und es auf die PET-Untersuchung bei Menschen zu übertragen, indem zusätzliche potenziell relevante Informationen mit Hilfe von maschinellem Lernen (ML) integriert werden und eine wohl etablierte pharmakokinetische Modellierungsmethode als Grundwahrheit verwendet wird.

Material und Methoden

Mausstudie: Sechs Mäuse nach photothrombotischem Schlaganfall (PT) und sechs Mäuse nach identischer Versuchsdurchführung, jedoch ohne Schlaganfall (sham), wurden in die Studie aufgenommen und mit einem dedizierten Kleintier-PET/MR-Scanner untersucht. Für die Hälfte der Mäuse wurden vier serielle Messungen 0-90 Minuten nach der Injektion (p.i.) pro Maus (Analysekohorte) durchgeführt und die TSPO_Bindung quantitativ geschätzt (Distribution Volume Ratio, DVR). Zusätzlich wurden semi-quantitative Schätzungen (Standardized Uptake Volume Ratio, SUVR) für fünf späte 10 min Zeitfenster berechnet. Wir verglichen die Eignung der SUVRs als Näherung für die DVR mittels linearer Anpassung und Pearson-Korrelationskoeffizient. Die andere Hälfte der Mäuse erhielt 60-90 min p.i. [^{18}F]GE-180-PET und wurde als Validierungskohorte verwendet. *Humanstudie*: 18 Probanden erhielten nach einem akuten ischämischen Schlaganfall 0-90 min p.i. [^{18}F]GE-180-PET zusammen mit einer Reihe von MRT-Sequenzen. Fünf manuelle venöse Blutproben wurden während des PET-Scans entnommen und ihre Aktivitätskonzentration gemessen. Auf der Grundlage der dynamischen PET-Daten wurde eine quantitative Schätzung der TSPO-Bindung voxelweise berechnet. Wir trainierten einen ML-Algorithmus, der diese Schätzungen als Grundwahrheit und drei späte 10 min PET-Bilder, das ASL-Bild, Voxelkoordinaten, die Läsionsmaske und die fünf Plasmaaktivitätskonzentrationen als Eingangsmerkmale verwendete. Unter Verwendung von Shapley Additive Explanations stellten wir fest, dass die drei späten PET-Bilder und die Plasmaaktivitätskonzentrationen den größten Einfluss auf die Qualität des Modells hatten. Anschließend testeten wir eine vereinfachte Quantifizierungsmethode, die darin bestand, ein spätes PET-Bild durch eine Plasmaaktivitätskonzentration zu dividieren. Alle Kombinationen von Bildern/Proben wurden anhand von Konkordanz-Korrelationskoeffizienten und Bland-Altman-Diagrammen verglichen.

Ergebnisse

Die Mausstudie zeigte, dass die 60-70, 70-80 und 80-90 min p.i. Zeitfenster die beste Näherung an die 90 min Scan basierte DVR sowohl bei den Sham- als auch bei den PT-Mäusen produzieren. Die Humanstudie zeigte auf der Basis individueller Voxel einen zusätzlichen Wert der späten Plasmaaktivitätskonzentration für die Näherung an die quantitative 90-min Scan-basierten TSPO-Schätzung. Die Division der Werte im 70-80 min p.i. Zeitfenster mit dem Messwert der 30 min p.i. Plasmaprobe ergab die genaueste semi-quantitative Schätzung in der ischämischen Läsion.

Schlussfolgerung

Eine zuverlässige vereinfachte TSPO-Quantifizierung bei Patienten nach einem akuten ischämischen Schlaganfall ist durch die Verwendung eines kurzen späten PET-Zeitfensters geteilt durch eine späte Plasmaaktivitätskonzentration möglich und kann somit eine vollständige Quantifizierung auf der Grundlage eines 90 min dynamischen Scans ersetzen. Das in dieser Arbeit verwendete ML-basierte Verfahren zur Schätzung der Relevanz verschiedener Merkmale kann in Zukunft auch für andere Erkrankungen und Tracer angewendet werden.

4. Abstract

Background

Ischemic stroke is the second leading cause of death and the third main cause of long-term disability worldwide, which explains the need for novel therapies to improve neurological recovery. Microglia, brain resident immune cells, are a suitable target for such a therapy. These cells express 18 kDa translocator protein (TSPO) when activated, which enables neuroinflammation monitoring using positron emission tomography (PET) with TSPO tracers, such as [^{18}F]GE-180. However, the signal in PET images originates not only from specific binding of the tracer to the receptor of interest; it is contaminated by non-specific binding and free tracer in both tissue and blood. Gold-standard quantification of [^{18}F]GE-180 specific binding is currently performed using pharmacokinetic modeling, which requires a longer scanning time and continuous arterial blood sampling. This is not only burdensome for the hospital staff, but also associated with additional risks and discomfort for the patient.

Aim

The aim of this work was to establish a simplified [^{18}F]GE-180 PET scanning protocol for a mouse ischemic stroke model and translate it into human PET by integrating additional potentially relevant information using machine learning (ML) and taking a well-established pharmacokinetic modeling method as the ground truth.

Materials and Methods

Mouse study: Six mice after photothrombotic stroke (PT) and six sham mice were included in the study and scanned using a dedicated small-animal PET/MR scanner. For a half of the mice, we acquired four serial 0–90 min post injection (p.i.) scans per mouse (analysis cohort) and calculated quantitative TSPO binding estimates (distribution volume ratio, DVR) as well as semi-quantitative estimates (standardized uptake volume ratio, SUVR) for five late 10 min time frames. We compared how well the obtained SUVRs approximated DVR by means of linear fitting and Pearson correlation coefficient. The other half of the mice received 60-90 min p.i. [^{18}F]GE-180 PET and was used as a validation cohort. *Human study:* 18 subjects after acute ischemic stroke received 0-90 min p.i. [^{18}F]GE-180 PET along with a number of MRI sequences. Five manual venous blood samples were drawn during the PET scan and their activity concentration was measured. Based on dynamic PET data, a quantitative TSPO binding estimate was calculated voxel-wise. We trained an ML algorithm using these estimates as the ground truth and three late 10 min PET frames, the ASL image, voxel coordinates, the lesion mask, and the five plasma activity concentrations as input features. Using Shapley Additive Explanations, we determined that the three late PET frames and the plasma activity concentrations had the highest impact on the model's performance. We then tested a simplified quantification approach consisting of dividing a late PET frame by a plasma activity concentration. All the combinations of frames/samples were compared by means of concordance correlation coefficient and Bland-Altman plots.

Results

The mouse study showed that the 60–70, 70–80, and 80–90 min p.i. frames produce the closest approximation for 90 min scan-based DVR in both sham and PT mice. The human study demonstrated on an individual voxel basis an additional value of the late plasma activity concentration in approximating the quantitative 90 min scan-based TSPO estimate. The 70-80 min p.i. frame divided by the 30 min p.i. plasma sample produced the closest semi-quantitative estimate in the ischemic lesion.

Conclusion

Reliable simplified TSPO quantification in patients after acute ischemic stroke is achievable by using a short late PET frame divided by a late plasma activity concentration and can thus replace full quantification based on a 90 min dynamic scan. The ML-based procedure of estimating feature importance used in this work can be applied for other conditions and other tracers in the future.

5. References

Akaike, H. (1974). A new look at the statistical model identification. *IEEE transactions on automatic control*, *19*(6), 716-723.

Albert, N. L., Unterrainer, M., Fleischmann, D., Lindner, S., Vettermann, F., Brunegraf, A., Vomacka, L., Brendel, M., Wenter, V., & Wetzel, C. (2017). TSPO PET for glioma imaging using the novel ligand 18F-GE-180: first results in patients with glioblastoma. *European journal of nuclear medicine and molecular imaging*, *44*(13), 2230-2238.

Boellaard, R., van Lingen, A., van Balen, S., Hoving, B. G., & Lammertsma, A. A. (2001). Characteristics of a new fully programmable blood sampling device for monitoring blood radioactivity during PET. *European journal of nuclear medicine*, *28*(1), 81-89.

Boutin, H., Murray, K., Pradillo, J., Maroy, R., Smigova, A., Gerhard, A., Jones, P. A., & Trigg, W. (2015). 18 F-GE-180: a novel TSPO radiotracer compared to 11 CR-PK11195 in a preclinical model of stroke. *European journal of nuclear medicine and molecular imaging*, *42*(3), 503-511.

Brackhan, M., Bascuñana, P., Ross, T. L., Bengel, F. M., Bankstahl, J. P., & Bankstahl, M. (2018). [18F] GE 180 positron emission tomographic imaging indicates a potential double-hit insult in the intrahippocampal kainate mouse model of temporal lobe epilepsy. *Epilepsia*, *59*(3), 617-626.

Buchert, R., Dirks, M., Schütze, C., Wilke, F., Mamach, M., Wirries, A.-K., Pflugrad, H., Hamann, L., Langer, L. B., & Wetzel, C. (2020). Reliable quantification of 18 F-GE-180 PET neuroinflammation studies using an individually scaled population-based input function or late tissue-to-blood ratio. *European journal of nuclear medicine and molecular imaging*, *47*(12), 2887-2900.

Buxton, R. B., Frank, L. R., Wong, E. C., Siewert, B., Warach, S., & Edelman, R. R. (1998). A general kinetic model for quantitative perfusion imaging with arterial spin labeling. *Magnetic resonance in medicine*, *40*(3), 383-396.

Chaney, A., Cropper, H. C., Johnson, E. M., Lechtenberg, K. J., Peterson, T. C., Stevens, M. Y., Buckwalter, M. S., & James, M. L. (2019). 11C-DPA-713 versus 18F-GE-180: a preclinical comparison of translocator protein 18 kDa PET tracers to visualize acute and chronic neuroinflammation in a mouse model of ischemic stroke. *Journal of Nuclear Medicine*, *60*(1), 122-128.

Cherry, S. R., Sorenson, J. A., & Phelps, M. E. (2012). *Physics in nuclear medicine e-Book*. Elsevier Health Sciences.

Deussing, M., Blume, T., Vomacka, L., Mahler, C., Focke, C., Todica, A., Unterrainer, M., Albert, N. L., Lindner, S., & von Ungern-Sternberg, B. (2018). Coupling between physiological TSPO expression in brain and myocardium allows stabilization of late-phase cerebral [18F] GE180 PET quantification. *Neuroimage*, *165*, 83-91.

Eriksson, L., Holte, S., Bohm, C., Kesselberg, M., & Hovander, B. (1988). Automated blood sampling systems for positron emission tomography. *IEEE Transactions on Nuclear Science*, *35*(1), 703-707.

Fan, Z., Calsolaro, V., Atkinson, R. A., Femminella, G. D., Waldman, A., Buckley, C., Trigg, W., Brooks, D. J., Hinz, R., & Edison, P. (2016). Flutriciclamide (18F-GE180) PET: first-in-human PET study of novel third-generation in vivo marker of human translocator protein. *Journal of Nuclear Medicine*, *57*(11), 1753-1759.

Fan, Z., Harold, D., Pasqualetti, G., Williams, J., Brooks, D. J., & Edison, P. (2015). Can studies of neuroinflammation in a TSPO genetic subgroup (HAB or MAB) be applied to the entire AD cohort? *Journal of Nuclear Medicine*, *56*(5), 707-713.

Feeney, C., Scott, G., Raffel, J., Roberts, S., Coello, C., Jolly, A., Searle, G., Goldstone, A., Brooks, D. J., & Nicholas, R. S. (2016). Kinetic analysis of the translocator protein positron emission tomography ligand [18 F] GE-180 in the human brain. *European journal of nuclear medicine and molecular imaging*, *43*(12), 2201-2210.

Feigin, V. L., Brainin, M., Norrving, B., Martins, S., Sacco, R. L., Hacke, W., Fisher, M., Pandian, J., & Lindsay, P. (2022). World Stroke Organization (WSO): global stroke fact sheet 2022. *International Journal of Stroke*, *17*(1), 18-29.

Ferré, J.-C., Bannier, E., Raoult, H., Mineur, G., Carsin-Nicol, B., & Gauvrit, J.-Y. (2013). Arterial spin labeling (ASL) perfusion: techniques and clinical use. *Diagnostic and interventional imaging*, *94*(12), 1211-1223.

Feske, S. K. (2021). Ischemic stroke. *The American Journal of Medicine*, *134*(12), 1457-1464.

Gerhard, A., Schwarz, J., Myers, R., Wise, R., & Banati, R. B. (2005). Evolution of microglial activation in patients after ischemic stroke: a [11C](R)-PK11195 PET study. *Neuroimage*, *24*(2), 591-595.

Gershen, L. D., Zanotti-Fregonara, P., Dustin, I. H., Liow, J.-S., Hirvonen, J., Kreisl, W. C., Jenko, K. J., Inati, S. K., Fujita, M., & Morse, C. L. (2015). Neuroinflammation in temporal lobe epilepsy measured using positron emission tomographic imaging of translocator protein. *JAMA neurology*, *72*(8), 882-888.

Guilarte, T. R. (2019). TSPO in diverse CNS pathologies and psychiatric disease: A critical review and a way forward. *Pharmacology & therapeutics*, *194*, 44-58.

Gulyás, B., Tóth, M., Schain, M., Airaksinen, A., Vas, Á., Kostulas, K., Lindström, P., Hillert, J., & Halldin, C. (2012). Evolution of microglial activation in ischaemic core and peri-infarct regions after stroke: a PET study with the TSPO molecular imaging biomarker [11C] vinpocetine. *Journal of the neurological sciences*, *320*(1-2), 110-117.

Gunn, R. N., Gunn, S. R., & Cunningham, V. J. (2001). Positron emission tomography compartmental models. *Journal of Cerebral Blood Flow & Metabolism*, *21*(6), 635-652.

Hastie, T., Tibshirani, R., Friedman, J. H., & Friedman, J. H. (2009). *The elements of statistical learning: data mining, inference, and prediction* (Vol. 2). Springer.

Herpich, F., & Rincon, F. (2020). Management of acute ischemic stroke. *Critical Care Medicine*, *48*(11), 1654.

Ho, T. K. (1995). Random decision forests. Proceedings of 3rd international conference on document analysis and recognition,

Holzgreve, A., Pötter, D., Brendel, M., Orth, M., Weidner, L., Gold, L., Kirchner, M. A., Bartos, L. M., Unterrainer, L. M., & Unterrainer, M. (2022). Longitudinal [18F] GE-180 PET Imaging Facilitates In Vivo Monitoring of TSPO Expression in the GL261 Glioblastoma Mouse Model. *Biomedicines*, *10*(4), 738.

Ido, T., Wan, C. N., Casella, V., Fowler, J., Wolf, A., Reivich, M., & Kuhl, D. (1978). Labeled 2-deoxy-D-glucose analogs. 18F-labeled 2-deoxy-2-fluoro-D-glucose, 2-deoxy-2-fluoro-D-mannose and 14C-2-deoxy-2-fluoro-D-glucose. *Journal of Labelled Compounds and Radiopharmaceuticals*, *14*(2), 175-183.

Ikawa, M., Lohith, T. G., Shrestha, S., Telu, S., Zoghbi, S. S., Castellano, S., Taliani, S., Da Settimo, F., Fujita, M., & Pike, V. W. (2017). 11C-ER176, a radioligand for 18-kDa translocator protein, has adequate sensitivity to robustly image all three affinity genotypes in human brain. *Journal of Nuclear Medicine*, *58*(2), 320-325.

Innis, R. B., Cunningham, V. J., Delforge, J., Fujita, M., Gjedde, A., Gunn, R. N., Holden, J., Houle, S., Huang, S.-C., & Ichise, M. (2007). Consensus nomenclature for in vivo imaging of reversibly binding radioligands. *Journal of Cerebral Blood Flow & Metabolism*, *27*(9), 1533-1539.

Kaiser, L., Holzgreve, A., Quach, S., Ingrisch, M., Unterrainer, M., Dekorsy, F. J., Lindner, S., Ruf, V., Brosch-Lenz, J., & Delker, A. (2022). Differential Spatial Distribution of TSPO or Amino Acid PET Signal and MRI Contrast Enhancement in Gliomas. *Cancers*, *14*(1), 53.

Knezevic, D., & Mizrahi, R. (2018). Molecular imaging of neuroinflammation in Alzheimer's disease and mild cognitive impairment. *Progress in Neuro-Psychopharmacology and Biological Psychiatry*, *80*, 123-131.

Koza, J. R., Bennett, F. H., Andre, D., & Keane, M. A. (1996). Automated design of both the topology and sizing of analog electrical circuits using genetic programming. In *Artificial intelligence in design'96* (pp. 151-170). Springer.

Kreisl, W. C., Jenko, K. J., Hines, C. S., Lyoo, C. H., Corona, W., Morse, C. L., Zoghbi, S. S., Hyde, T., Kleinman, J. E., & Pike, V. W. (2013). A genetic polymorphism for translocator protein 18 kDa affects both in vitro and in vivo radioligand binding in human brain to this putative biomarker of neuroinflammation. *Journal of Cerebral Blood Flow & Metabolism*, *33*(1), 53-58.

Krupinski, J., Kaluza, J., Kumar, P., & Kumar, S. (1996). Immunocytochemical studies of cellular reaction in human ischemic brain stroke. MAB anti-CD68 stains macrophages, astrocytes and microglial cells in infarcted area. *Folia Neuropathologica*, *34*(1), 17-24.

Kuttner, S., Wickstrøm, K. K., Kalda, G., Dorraji, S. E., Martin-Armas, M., Oteiza, A., Jenssen, R., Fenton, K., Sundset, R., & Axelsson, J. (2020). Machine learning derived input-function in a dynamic 18F-FDG PET study of mice. *Biomedical Physics & Engineering Express*, *6*(1), 015020.

Kuttner, S., Wickstrøm, K. K., Lubberink, M., Tolf, A., Burman, J., Sundset, R., Jenssen, R., Appel, L., & Axelsson, J. (2021). Cerebral blood flow measurements with 15O-water PET using a non-invasive machine-learning-derived arterial input function. *Journal of Cerebral Blood Flow & Metabolism*, *41*(9), 2229-2241.

Lavisse, S., Guillermier, M., Hérard, A.-S., Petit, F., Delahaye, M., Van Camp, N., Haim, L. B., Lebon, V., Remy, P., & Dollé, F. (2012). Reactive astrocytes overexpress TSPO and are detected by TSPO positron emission tomography imaging. *Journal of Neuroscience*, *32*(32), 10809-10818.

Liu, B., Le, K. X., Park, M.-A., Wang, S., Belanger, A. P., Dubey, S., Frost, J. L., Holton, P., Reiser, V., & Jones, P. A. (2015). In vivo detection of age-and disease-related increases in neuroinflammation by 18F-GE180 TSPO microPET imaging in wild-type and Alzheimer's transgenic mice. *Journal of Neuroscience*, *35*(47), 15716-15730.

Logan, J., Fowler, J. S., Volkow, N. D., Wolf, A. P., Dewey, S. L., Schlyer, D. J., MacGregor, R. R., Hitzemann, R., Bendriem, B., & Gatley, S. J. (1990). Graphical analysis of reversible radioligand binding from time—activity measurements applied to [N-11C-methyl]-(−)-cocaine PET studies in human subjects. *Journal of Cerebral Blood Flow & Metabolism*, *10*(5), 740-747.

López-Picón, F. R., Snellman, A., Eskola, O., Helin, S., Solin, O., Haaparanta-Solin, M., & Rinne, J. O. (2018). Neuroinflammation appears early on PET imaging and then plateaus in a mouse model of Alzheimer disease. *Journal of Nuclear Medicine*, *59*(3), 509-515.

Lundberg, S. M., & Lee, S.-I. (2017). A unified approach to interpreting model predictions. *Advances in neural information processing systems*, *30*.

Ma, Y., Wang, J., Wang, Y., & Yang, G.-Y. (2017). The biphasic function of microglia in ischemic stroke. *Progress in neurobiology*, *157*, 247-272.

Madinier, A., Bertrand, N., Mossiat, C., Prigent-Tessier, A., Beley, A., Marie, C., & Garnier, P. (2009). Microglial involvement in neuroplastic changes following focal brain ischemia in rats. *PloS one*, *4*(12), e8101.

Mahler, C., Schumacher, A.-M., Unterrainer, M., Kaiser, L., Höllbacher, T., Lindner, S., Havla, J., Ertl-Wagner, B., Patzig, M., & Seelos, K. (2021). TSPO PET imaging of natalizumab-associated progressive multifocal leukoencephalopathy. *Brain*, *144*(9), 2683-2695.

Maimon, O. Z., & Rokach, L. (2014). *Data mining with decision trees: theory and applications* (Vol. 81). World scientific.

Morris, E. D., Endres, C. J., Schmidt, K. C., Christian, B. T., Muzic, R. F., & Fisher, R. E. (2004). Kinetic modeling in positron emission tomography. *Emission tomography*, *46*, 499-540.

Morris, R. S., Simon Jones, P., Alawneh, J. A., Hong, Y. T., Fryer, T. D., Aigbirhio, F. I., Warburton, E. A., & Baron, J.-C. (2018). Relationships between selective neuronal loss and microglial activation after ischaemic stroke in man. *Brain*, *141*(7), 2098-2111.

Moskowitz, M. A., Lo, E. H., & Iadecola, C. (2010). The science of stroke: mechanisms in search of treatments. *Neuron*, *67*(2), 181-198.

Mourik, J. E., Lubberink, M., Schuitemaker, A., Tolboom, N., van Berckel, B. N., Lammertsma, A. A., & Boellaard, R. (2009). Image-derived input functions for PET brain studies. *European journal of nuclear medicine and molecular imaging*, *36*(3), 463-471.

Nakajima, K., & Kohsaka, S. (2004). Microglia: neuroprotective and neurotrophic cells in the central nervous system. *Current Drug Targets-Cardiovascular & Hematological Disorders*, *4*(1), 65-84.

Nogueira, R. G., Jadhav, A. P., Haussen, D. C., Bonafe, A., Budzik, R. F., Bhuva, P., Yavagal, D. R., Ribo, M., Cognard, C., & Hanel, R. A. (2018). Thrombectomy 6 to 24 hours after stroke with a mismatch between deficit and infarct. *New England Journal of Medicine*, *378*(1), 11-21.

Pan, L., Cheng, C., Haberkorn, U., & Dimitrakopoulou-Strauss, A. (2017). Machine learning-based kinetic modeling: a robust and reproducible solution for quantitative analysis of dynamic PET data. *Physics in Medicine & Biology*, *62*(9), 3566.

Papadopoulos, V., Baraldi, M., Guilarte, T. R., Knudsen, T. B., Lacapère, J.-J., Lindemann, P., Norenberg, M. D., Nutt, D., Weizman, A., & Zhang, M.-R. (2006). Translocator protein (18 kDa): new nomenclature for the peripheral-type benzodiazepine receptor based on its structure and molecular function. *Trends in pharmacological sciences*, *27*(8), 402-409.

Pauwels, E., Ribeiro, M., Stoot, J., McCready, V., Bourguignon, M., & Maziere, B. (1998). FDG accumulation and tumor biology. *Nuclear medicine and biology*, *25*(4), 317-322.

Polikar, R. (2006). Ensemble based systems in decision making. *IEEE Circuits and systems magazine*, *6*(3), 21-45.

Powers, W. J. (2020). Acute ischemic stroke. *New England Journal of Medicine*, *383*(3), 252-260.

Price, C. J., Wang, D., Menon, D. K., Guadagno, J. V., Cleij, M., Fryer, T., Aigbirhio, F., Baron, J.-C., & Warburton, E. A. (2006). Intrinsic activated microglia map to the peri-infarct zone in the subacute phase of ischemic stroke. *Stroke*, *37*(7), 1749-1753.

Qiao, L., Fisher, E., McMurray, L., Milicevic Sephton, S., Hird, M., Kuzhuppilly-Ramakrishnan, N., Williamson, D. J., Zhou, X., Werry, E., & Kassiou, M. (2019). Radiosynthesis of (R, S)-[18F] GE387: A Potential PET Radiotracer for Imaging Translocator Protein 18 kDa (TSPO) with Low Binding Sensitivity to the Human Gene Polymorphism rs6971. *ChemMedChem*, *14*(9), 982-993.

Ribeiro, M. T., Singh, S., & Guestrin, C. (2016). " Why should i trust you?" Explaining the predictions of any classifier. Proceedings of the 22nd ACM SIGKDD international conference on knowledge discovery and data mining,

Russell, S. J. (2010). *Artificial intelligence a modern approach*. Pearson Education, Inc.

Russmann, V., Brendel, M., Mille, E., Helm-Vicidomini, A., Beck, R., Günther, L., Lindner, S., Rominger, A., Keck, M., & Salvamoser, J. D. (2017). Identification of brain regions predicting epileptogenesis by serial [18F] GE-180 positron emission tomography imaging of neuroinflammation in a rat model of temporal lobe epilepsy. *NeuroImage: Clinical*, *15*, 35-44.

Schuster, S., Beyer, L., Palleis, C., Harris, S., Schmitt, J., Weidinger, E., Prix, C., Bötzel, K., Danek, A., & Rauchmann, B.-S. (2022). Impact of Partial Volume Correction on [18F] GE-180 PET Quantification in Subcortical Brain Regions of Patients with Corticobasal Syndrome. *Brain Sciences*, *12*(2), 204.

Seo, H., Badiei Khuzani, M., Vasudevan, V., Huang, C., Ren, H., Xiao, R., Jia, X., & Xing, L. (2020). Machine learning techniques for biomedical image segmentation: an overview of technical aspects and introduction to state-of-art applications. *Medical physics*, *47*(5), e148-e167.

Setiawan, E., Wilson, A. A., Mizrahi, R., Rusjan, P. M., Miler, L., Rajkowska, G., Suridjan, I., Kennedy, J. L., Rekkas, P. V., & Houle, S. (2015). Role of translocator protein density, a

marker of neuroinflammation, in the brain during major depressive episodes. *JAMA psychiatry*, *72*(3), 268-275.

Shapley, L. S. (1997). A value for n-person games. *Classics in game theory*, *69*.

Stoll, G., Jander, S., & Schroeter, M. (1998). Inflammation and glial responses in ischemic brain lesions. *Progress in neurobiology*, *56*(2), 149-171.

Sucksdorff, M., Rissanen, E., Tuisku, J., Nuutinen, S., Paavilainen, T., Rokka, J., Rinne, J., & Airas, L. (2017). Evaluation of the effect of fingolimod treatment on microglial activation using serial PET imaging in multiple sclerosis. *Journal of Nuclear Medicine*, *58*(10), 1646-1651.

Suppiah, S., Didier, M.-A., & Vinjamuri, S. (2019). The who, when, why, and how of PET amyloid imaging in management of Alzheimer's disease—Review of literature and interesting images. *Diagnostics*, *9*(2), 65.

Thiel, A., & Heiss, W.-D. (2011). Imaging of microglia activation in stroke. *Stroke*, *42*(2), 507-512.

Thiel, A., Radlinska, B. A., Paquette, C., Sidel, M., Soucy, J.-P., Schirrmacher, R., & Minuk, J. (2010). The temporal dynamics of poststroke neuroinflammation: a longitudinal diffusion tensor imaging–guided PET study with 11C-PK11195 in acute subcortical stroke. *Journal of Nuclear Medicine*, *51*(9), 1404-1412.

Tiwari, A. K., Fujinaga, M., Yui, J., Yamasaki, T., Xie, L., Kumata, K., Mishra, A. K., Shimoda, Y., Hatori, A., & Ji, B. (2014). Synthesis and evaluation of new 18 F-labelled acetamidobenzoxazolone-based radioligands for imaging of the translocator protein (18 kDa, TSPO) in the brain. *Organic & Biomolecular Chemistry*, *12*(47), 9621-9630.

Tomimoto, H., Akiguchi, I., Wakita, H., Kinoshita, A., Ikemoto, A., Nakamura, S., & Kimura, J. (1996). Glial expression of cytokines in the brains of cerebrovascular disease patients. *Acta neuropathologica*, *92*(3), 281-287.

Unterrainer, M., Fleischmann, D., Vettermann, F., Ruf, V., Kaiser, L., Nelwan, D., Lindner, S., Brendel, M., Wenter, V., & Stöcklein, S. (2020). TSPO PET, tumour grading and molecular genetics in histologically verified glioma: A correlative 18F-GE-180 PET study. *European journal of nuclear medicine and molecular imaging*, *47*(6), 1368-1380.

Unterrainer, M., Mahler, C., Vomacka, L., Lindner, S., Havla, J., Brendel, M., Böning, G., Ertl-Wagner, B., Kümpfel, T., & Milenkovic, V. (2018). TSPO PET with [18F] GE-180 sensitively detects focal neuroinflammation in patients with relapsing–remitting multiple sclerosis. *European journal of nuclear medicine and molecular imaging*, *45*(8), 1423-1431.

Vandenberghe, R., Nelissen, N., Salmon, E., Ivanoiu, A., Hasselbalch, S., Andersen, A., Korner, A., Minthon, L., Brooks, D. J., & Van Laere, K. (2013). Binary classification of 18F-flutemetamol PET using machine learning: comparison with visual reads and structural MRI. *Neuroimage*, *64*, 517-525.

Vettermann, F. J., Harris, S., Schmitt, J., Unterrainer, M., Lindner, S., Rauchmann, B.-S., Palleis, C., Weidinger, E., Beyer, L., & Eckenweber, F. (2021). Impact of TSPO Receptor Polymorphism on [18F] GE-180 Binding in Healthy Brain and Pseudo-Reference Regions of Neurooncological and Neurodegenerative Disorders. *Life*, *11*(6), 484.

Vivash, L., & O'Brien, T. J. (2016). Imaging microglial activation with TSPO PET: lighting up neurologic diseases? *Journal of Nuclear Medicine*, *57*(2), 165-168.

Vomacka, L., Albert, N. L., Lindner, S., Unterrainer, M., Mahler, C., Brendel, M., Ermoschkin, L., Gosewisch, A., Brunegraf, A., & Buckley, C. (2017). TSPO imaging using the novel PET ligand [18 F] GE-180: quantification approaches in patients with multiple sclerosis. *EJNMMI research*, *7*(1), 1-9.

Wadsworth, H., Jones, P. A., Chau, W.-F., Durrant, C., Fouladi, N., Passmore, J., O'Shea, D., Wynn, D., Morisson-Iveson, V., & Ewan, A. (2012). [18F] GE-180: a novel fluorine-18 labelled PET tracer for imaging translocator protein 18 kDa (TSPO). *Bioorganic & medicinal chemistry letters*, *22*(3), 1308-1313.

Wang, G., Ye, J. C., & De Man, B. (2020). Deep learning for tomographic image reconstruction. *Nature Machine Intelligence*, *2*(12), 737-748.

Wang, T., Lei, Y., Fu, Y., Curran, W. J., Liu, T., Nye, J. A., & Yang, X. (2020). Machine learning in quantitative PET: A review of attenuation correction and low-count image reconstruction methods. *Physica Medica*, *76*, 294-306.

Watabe, H., Ikoma, Y., Kimura, Y., Naganawa, M., & Shidahara, M. (2006). PET kinetic analysis—compartmental model. *Annals of nuclear medicine*, *20*(9), 583-588.

Weishaupt, D., & Köchli, V. (2009). Borut Marincek. Wie funktioniert MRI. In: Heidelberg: Springer Medizin Verlag.

Werry, E. L., Bright, F. M., Piguet, O., Ittner, L. M., Halliday, G. M., Hodges, J. R., Kiernan, M. C., Loy, C. T., Kril, J. J., & Kassiou, M. (2019). Recent developments in TSPO PET imaging as a biomarker of neuroinflammation in neurodegenerative disorders. *International journal of molecular sciences*, *20*(13), 3161.

Wimberley, C., Nguyen, D. L., Truillet, C., Peyronneau, M.-A., Gulhan, Z., Tonietto, M., Boumezbeur, F., Boisgard, R., Chalon, S., & Bouilleret, V. (2020). Longitudinal mouse-PET imaging: a reliable method for estimating binding parameters without a reference region or blood sampling. *European journal of nuclear medicine and molecular imaging*, *47*(11), 2589-2601.

Zanotti-Fregonara, P., Pascual, B., Rizzo, G., Yu, M., Pal, N., Beers, D., Carter, R., Appel, S. H., Atassi, N., & Masdeu, J. C. (2018). Head-to-head comparison of 11C-PBR28 and 18F-GE180 for quantification of the translocator protein in the human brain. *Journal of Nuclear Medicine*, *59*(8), 1260-1266.

Zhang, L., Hu, K., Shao, T., Hou, L., Zhang, S., Ye, W., Josephson, L., Meyer, J. H., Zhang, M.-R., & Vasdev, N. (2021). Recent developments on PET radiotracers for TSPO and their applications in neuroimaging. *Acta Pharmaceutica Sinica B*, *11*(2), 373-393.

6. Paper I

The first article appeared in *Frontiers in Medicine* in 2022 and can be found with the following reference:

Zatcepin, A., Heindl, S., Schillinger, U., Kaiser, L., Lindner, S., Bartenstein, P., Kopczak, A., Liesz, A., Brendel, M., & Ziegler, S. I. (2022). Reduced Acquisition Time [18F] GE-180 PET Scanning Protocol Replaces Gold-Standard Dynamic Acquisition in a Mouse Ischemic Stroke Model. *Frontiers in Medicine*, *9*.

DOI: 10.3389/fmed.2022.830020

7. Paper II

The second article was accepted by *Zeitschrift für medizinische Physik* in 2022, appeared in this journal in 2023, and can be found with the following reference:

Zatcepin, A., Kopczak, A., Holzgreve, A., Hein, S., Schindler, A., Duering, M., Kaiser, L., Lindner, S., Schidlowski, M., Bartenstein, P., Albert, N., Brendel, M., & Ziegler, S. I. (2023). Machine learning-based approach reveals essential features for simplified TSPO PET quantification in ischemic stroke patients. *Z Med Phys*.

DOI: 10.1016/j.zemedi.2022.11.008

Danksagung

Als Erstes möchte ich mich bei meiner Betreuerin und einer wunderbaren Person Prof. Dr. Sibylle Ziegler bedanken, deren Anleitung mir diese Arbeit ermöglicht hat. Trotz ihres vollen Terminkalenders fand Prof. Ziegler jede Woche Zeit, um mein Projekt zu besprechen und war immer für mich da, wenn ich ihre Hilfe brauchte. Als Person mit großem Fachwissen hat sie mir nicht nur unzählige Dinge über die PET-Physik beigebracht, sondern auch mein Interesse für dieses erstaunliche Fachgebiet geweckt. Vielen Dank, Prof. Ziegler, für die Korrekturen von meinen Manuskripten, großartige wissenschaftliche Diskussionen, Motivation und Glauben an mich. Ich fühle mich geehrt und schätze mich sehr glücklich, Sie meine Doktormutter genannt haben zu dürfen.

Ganz herzlich bedanke ich mich bei PD Dr. Matthias Brendel, der meine Arbeit während der gesamten Promotionszeit von medizinischer Seite mitbetreut hat. Als Autor zahlreicher wissenschaftlicher Arbeiten und als Experte für wissenschaftliches Schreiben hat Matthias mir viel beigebracht, indem er meine Entwürfe für Vorträge und Kongress-Zusammenfassungen gelesen und korrigiert hat. Ich hatte das Glück, mit Matthias an dem Mikroglia-Synchronisationsprojekt zu arbeiten, das mich dazu motivierte, mehr über die Alzheimer-Krankheit und die molekulare Connectivity zu erfahren, und mir die Möglichkeit gab, auf mehreren Kongressen Vorträge zu halten, und zu einem großartigen Manuskript führte.

Ich möchte mich bei Dr. Anna Kopczak aus dem ICARUS-Team bedanken, die die Patientenrekrutierung und die MR-Scans durchgeführt und die zweite Arbeit dieser Dissertation ermöglicht hat. Anna, es war eine Freude, mit Dir zusammenzuarbeiten, und ich danke Dir für Deine Hilfe mit dem Manuskript.

Ich bedanke mich auch bei Dr. Steffanie Heindl und Dr. Ulrike Schillinger für die Tier-Scans, die im ersten Paper von dieser Dissertation verwendet wurden. Darüber hinaus gilt ein großer Dank auch dem gesamten ICARUS-Team und allen Ko-Autoren von den beiden Manuskripten.

Mein besonderer Dank gilt Andreas Bollenbacher, Isabella Berg, Birkan Secgin, Sophie Kunte, Letizia Vogler und Dr. Maximilian Scheifele für die Durchführung der PET-Scans und die Entnahme der Blutproben.

Ich möchte mich bei Herrn Prof. Dr. Peter Bartenstein, der Leiter unserer Abteilung, für die Möglichkeit, an diesem großartigen Projekt zu arbeiten, bedanken. Die in dieser Dissertation dargestellte Arbeit wurde von der Deutschen Forschungsgemeinschaft gefordert, der ich an dieser Stelle auch danken möchte.

Ein großer Dank gilt meinem ehemaligen Kollegen Dr. Maximilian Grosch, der während meiner Promotion auch mein guter Freund geworden ist. Max hat mir während meines ersten Jahres sehr geholfen: er hat für mich die Welt des PMOD entdeckt, hat mich motiviert, meine Fähigkeiten in Python zu verbessern und hat mir viel über metabolische Konnektivität zusammen mit einer Menge Schwäbisch beigebracht. *Schaffe, schaffe, Häusle baue* ist zu meinem Motto geworden und hat für den zügigen Ablauf meiner Promotion gesorgt.

Dr. Lena Kaiser ist eine weitere Kollegin, bei der ich mich bedanken möchte. Lena hat mich mit der kinetischen Modellierung in PET vertraut gemacht und mir dabei und bei allen Fragen zu GE180 geholfen. Von Lena habe ich auch viel über die Arbeit in PMOD und MITK gelernt.

Ein weiterer Kollege und enger Freund, bei dem ich mich bedanken möchte, ist Adrian Zounek. Mit Adi habe ich während meiner Promotion nicht nur viele Diskussionen über künstliche Intelligenz und Statistik geführt, sondern auch viel Spaß gehabt. Die Kongresse in Leipzig und Barcelona, die Radiomics School in Wien wären ohne ihn nicht dasselbe gewesen. Danke Dir für die Blutmessungen während meines Urlaubs und für die Hilfe mit der deutschen Übersetzung der Zusammenfassung dieser Dissertation.

Ich bin all meinen Kolleginnen und Kollegen von der NUK sehr dankbar. Es war eine Freude, in einem so freundlichen, unterstützenden und lustigen Team zu arbeiten. Außerdem verdanke ich dem NUK-Team meine großen Fortschritte in Deutsch.